Scaling Laws Applied to a Modal Formulation of the Aeroservoelastic Equations

Anthony S. Pototzky
NASA Langley Research Center
Hampton, Virginia

ABSTRACT

A method of scaling is described that easily converts the aeroelastic equations of motion of a full-sized aircraft into ones of a wind-tunnel model. To implement the method, a set of rules is provided for the conversion process involving matrix operations with scale factors. In addition, a technique for analytically incorporating a spring mounting system into the aeroelastic equations is also presented. As an example problem, a finite element model of a full-sized aircraft is introduced from the High Speed Research (HSR) program to exercise the scaling method. With a set of scale factor values, a brief outline is given of a procedure to generate the first-order aeroservoelastic analytical model representing the wind-tunnel model. To verify the scaling process as applied to the example problem, the root-locus patterns from the full-sized vehicle and the wind-tunnel model are compared to see if the root magnitudes scale with the frequency scale factor value. Selected time-history results are given from a numerical simulation of an active-controlled wind-tunnel model to demonstrate the utility of the scaling process.

Introduction

The effort to develop the scaling method that is the subject matter of this paper began in 1997 during the latter part of the NASA-sponsored High Speed Research (HSR) program. During this time period, the Technical Concept Aircraft (TCA) shown in Figure 1 was being studied. The HSR program dealt with several aeroelastic issues associated with this configuration. For example, the aeroelastic behavior of the TCA is dominated by its low-frequency structural modes. These low-frequency modes and the vibrations they cause, particularly throughout the fuselage area, impact the pilot's ability to fly the aircraft, passenger comfort and the design of the flight control system. To address the issues of cockpit vibrations and passenger comfort, a small, actively-controlled, ride-control vane (rcv) was incorporated near the pilot station later in the design of the aircraft. Its function was to reduce low-frequency vibrations mainly at the pilot station while minimally impacting the flight control system.

A related aeroelastic issue was to stabilize, within the aircraft's flight envelope, a critical flutter mode involving the highly coupled motion of the massive outboard engine pod that was supported by a pylon aft of the main wing spar. With much effort, this task was accomplished by aeroelastically tailoring the structure primarily in the wing area. In spite of this tailoring effort, there was concern that this flutter mode might reappear at some point later in the HSR program, either from the inherent differences between the physical and idealized structure of the aircraft or from some nonlinear aerodynamic effects at transonic speeds. Should this problem have arisen, the use of active controls was identified as a reasonable solution to augment stability or alleviate this or other flutter problems.

Both control system and aeroelastic issues were studied by performing analyses and real-time flight simulations. Although these studies produced encouraging results, there are still many questions that are difficult or impossible to answer solely with these "paper" studies. For example, are control system stability, cross-coupling, and flutter mechanisms affected by nonlinear aerodynamics at transonic speeds? Such questions can only be answered early in the aircraft's design phase by conducting wind-tunnel tests of actively controlled, scaled aeroelastic models.

Designing and building actively-controlled aeroelastic wind-tunnel models is a time-consuming, complex, and costly process. All the elements for designing a wind-tunnel model for successful wind-tunnel testing need to be in place before the physical model can be built. Developing and analyzing a wind-tunnel *analytical* model first is a good way to develop and validate all the necessary elements that go into designing, building and testing a *physical* wind-tunnel model.

In terms of actively controlled wind-tunnel models, analytical models can be used to identify control surface and sensor locations that will maximize control law objectives and minimize control system cross-coupling. Analytical models can also be used to design control laws for improving ride quality, augmenting flutter stability, setting model attitudes, and alleviating gust loads. Valuable insight into the design and testing of active-controlled physical models can be gained through

closed-loop simulations using the analytical model. The analytical model can also be used to identify the open-loop and closed-loop flutter boundaries at the test conditions of interest.

When an actively-controlled aeroelastic wind-tunnel model is not a scaled representation of a full-scale vehicle, an approach that has been used in the past is first to design and build a physical wind-tunnel model and then to develop a finite element model (FEM) based on the physical model (Ref. 1).

If a detailed finite element model of a full-sized aircraft were available, another approach based on a replica scaling has also been used for developing a wind-tunnel model. The dashed lines in the flow diagram of Figure 2 show the path for this approach. This approach encompasses directly applying appropriate scale factors to thousands of entries in a large and detailed finite element model. Applying this approach is a very time-consuming process and, if composite materials are used in the design of the aircraft, scaling can additionally become a very complicated process. However, this approach has the advantage of producing a scaled finite element model for directly generating a wind-tunnel analytical model and for designing a physical wind-tunnel model.

If the wind-tunnel model is in the planning stages of development and a scaled finite element model is not immediately needed, the path indicated by the solid lines in Figure 2 shows a more efficient approach. With this approach, the wind-tunnel aeroelastic EOM can be generated by scaling the full-sized aircraft aeroelastic EOM. While engaged in the HSR program, this author identified this approach in the aeroelastic analyses of the TCA. This approach is the main contribution of this paper.

This approach is especially attractive since it requires the computation of significantly smaller matrices, it requires much simpler scaling rules, and it avoids scaling the much larger FEM with complicated scaling rules. Nevertheless, the proposed approach for generating aeroelastic EOM requires MSC.Nastran (Ref. 2) to perform an Aeroelastic Response Analysis of the full-sized finite element model and DMAP (Direct Matrix Abstraction Programming, Ref. 3) to access and output the appropriate matrices for the scaling process.

The paper begins with the implementation section that describes the underlying assumptions, the scale factors, and the computational rules for scaling the matrices comprising the aeroelastic equations of motion. The next section briefly describes the s-plane procedure for fitting the frequency-dependent generalized aerodynamic force coefficients (GAF). Also in this section, a technique is presented to modify open-loop aeroservoelastic (ASE) equations with a term to represent a wind-tunnel model spring-mounting system. The last section introduces the TCA finite element model that exercises the scaling procedure. There is a discussion on the scale factor values used in the scaling procedure and also the sizes and pertinent flutter parameters for both the aircraft and model. The discussion continues by briefly outlining the procedures used to generate and output the aeroelastic modal matrices needed for the scaling process. Next, to verify scaling process, root locus results are presented of the full and scaled, open-loop aeroelastic equations generated by Matlab (Ref. 4). Next, a Simulink model (Ref. 5) incorporating the open-loop ASE model with flutter suppression and ride quality control laws is introduced to demonstrate the closed loop system. Finally, open-loop and closed-loop time-history results using Simulink are presented to complete the demonstration.

Implementation of the Scaling Method

The scaling factors used in this paper follow from the similarity laws described in Reference 6 and are given in Table 1. As is customary in Mach scaled flutter models, the assumption is made that reduced frequency, mass ratio, and Mach number have the same values for both the full-sized and scaled analytical models. The length, velocity, and dynamic pressure scale factors in Table 1 are selected as the primary scale factors and all other scaling factors are derived from them, as indicated by the equations in the table.

The general form of the aeroelastic equation of motion with control and gust inputs is given by

$$\left[-w^2 M + M\left(\left[ig\right] + I\right)\left[(2pf_n)^2\right] + \bar{q}Q(ik)\right]\{q\} - w^2 M_c q_c + \bar{q}Q_c(ik)q_c + \bar{q}Q_g(ik)w_g = 0 \qquad (1)$$

This equation is similar to the "aeroelastic response equation" given in the Aeroelastic Analysis Users Guide of MSC.Nastran in Reference 3. This form of the equation ignores the hinge moment terms, since the hinge moment aerodynamics are assumed to be negligible compared to the moment produced by the actuator. In the above equation, the quantities M and M_c are the generalized modal mass matrices of the structure and the control surfaces, respectively, of the full-sized aircraft. In equation (1), the generalized modal stiffness and structural damping matrices are represented by the quantities $M\left[(2pf_n)^2\right]$ and $M\left[ig\right]\left[(2pf_n)^2\right]$, respectively. The quantities $Q(ik)$, $Q_c(ik)$ and $Q_g(ik)$ are the reduced-frequency-dependent generalized aerodynamic force (GAF) matrices of the full-sized aircraft due to vehicle motion, control surface deflections, and gust, respectively. The quantity $\bar{q}$ is the

dynamic pressure. Also in equation (1), the quantities q and q_c are the generalized displacement vectors for the flexible modes motion and the control surface input motion, respectively. The quantity w_g is the gust velocity input. The reduced and angular frequencies are represented by the quantities k and w, respectively.

The following equations define the rotational and translational sensor output quantities:

$$r = F_r q \quad (2)$$

$$z = F_d q \quad (3)$$

respectively. The quantities F_r and F_d are the modal deflection matrices for rotation and translation at the various sensor locations on the structure.

In this paper, space limitations prevent giving derivations of all the scaling rules; although many of the scaling rules are straightforward and need little explanation. In what follows, the helpful explanations are given where needed for some of the more subtle applications of the scaling rules.

The matrices in equation (1) are multiplied by the appropriate scale factors appearing in Table 1 to obtain the matrices needed to form the symmetrical equations of motion of the wind-tunnel model. The generalized modal mass matrix, M, is scaled by multiplying the matrix elements as follows:

$$M_{wtm} = s_l \rightarrow \overbrace{\begin{bmatrix} M\,of\,Plungerowcol & & \\ & M\,of\,Pitchrowcol & \\ & & M\,of\,Flexmodes \end{bmatrix}}^{s_m} \uparrow s_l \quad (4)$$

In equation 4, the bracket and arrows are shown to indicate the pattern of the multiplication operations applied to the matrix elements. The horizontal bracket extending over the entire matrix signifies an operation where all the elements in that matrix are multiplied by the mass scale factor. The arrows pointing to a row and a column signify additional operations wherein all the elements in that row and then all the elements in that column are multiplied by the length scale factor. This notation is used in the remainder of the paper to describe the matrix element multiplication operations with the various scale factors.

Since the control surfaces involve rigid-body rotations about hinge lines, the elements of the control surface generalized mass matrix are multiplied by both s_l and s_m as follows:

$$M_{c\,wtm} = s_l \rightarrow \overbrace{\begin{bmatrix} M_c\,of\,Plungerow \\ M_c\,of\,Pitchrow \\ M_c\,of\,Flexmodes \end{bmatrix}}^{s_l \times s_m} \quad (5)$$

The natural frequencies are multiplied by s_f according to

$$\{f_{n\,wtm}\} = s_f \{f_n\} \quad (6)$$

The GAF matrix, $Q(ik)$, and the other GAF matrices are multiplied by s_l to scale a length dimension in the span direction implicit in the GAF coefficient in every element. As was done for the generalized mass matrix, the pitch row and column elements are separately scaled again by s_l.

$$Q_{wtm}(ik) = s_l \rightarrow \overbrace{\begin{bmatrix} Q(ik)\,of\,Plungerowcol & & \\ & Q(ik)\,of\,Pitchrowcol & \\ & & Q(ik)\,of\,Flexmodes \end{bmatrix}}^{s_l} \uparrow s_l \quad (7)$$

The control surface GAF matrix is scaled as follows:

$$Q_{c\,wtm}(ik) = s_l \rightarrow \overbrace{\begin{bmatrix} Q_c(ik)\,of\,Plungerow \\ Q_c(ik)\,of\,Pitchrow \\ Q_c(ik)\,of\,Flexmodes \end{bmatrix}}^{s_l^2} \quad (8)$$

The gust GAF matrix scaling matches control surface GAF matrix scaling,,

$$Q_{g\,wtm}(ik) = s_l \rightarrow \overbrace{\begin{bmatrix} Q_g(ik)\,of\,Plungerow \\ Q_g(ik)\,of\,Pitchrow \\ Q_g(ik)\,of\,Flexmodes \end{bmatrix}}^{s_l^2} \quad (9)$$

To assure that the aerodynamic transport lag times are correctly scaled to model size, the reference length used in computing reduced frequency needs to be multiplied by the length scale factor, s_l.

$$cref_{wtm} = cref * s_l \tag{10}$$

The scaling applied to the generalized modal mass matrix automatically provides the proper scaling of all the vibration mode shape deflections. Since the generalized mass corresponding to the pitch row and column is multiplied by the length scale factor, the pitch column elements of the translational sensor deflection matrix must also be multiplied by,

$$F_{d\ wtm} = \begin{bmatrix} F_d\ of\ plungecol & \overset{s_l}{\downarrow} & F_d\ of\ flexmodes \\ \vdots & F_d\ of\ pitchcol & \vdots \\ & \vdots & \end{bmatrix} \tag{11}$$

An expression for scaling the rotational sensor deflection matrix can be deduced by noting that the derivative of the translational deflection component of a mode shape is the rotational deflection and is given by dz/dx. If the elements of the rotational sensor deflection matrix are defined in terms of derivatives, then the scaling of the elements is achieved by applying the length scale factor to the denominator of the derivative, i.e., dz / ($dx_* s_l$). Based on these considerations, the scale factor of $1/s_l$ multiplies all the rotational deflection elements. The rotational sensor deflection matrix is scaled as follows:

$$F_{r\ wtm} = \begin{bmatrix} F_r\ of\ plungecol & \overbrace{\quad}^{1/s_l} & F_r\ of\ flexmodes \\ \vdots & F_r\ of\ pitchcol & \vdots \\ & \vdots & \\ & \underset{s_l}{\uparrow} & \end{bmatrix} \tag{12}$$

In the above matrix, the plunge elements in the first column are all zeros since the spatial derivative of the plunge mode is zero. The adjacent pitch column elements are effectively multiplied by unity because the two scale factors are inverses of one another.

Analytical Model

The s-Plane Fit of the GAF Coefficients

To model the first-order state-space form of the aeroservoelastic equation, s-plane unsteady aerodynamics is required. Using the scaled GAFs defined in the frequency domain, the fitting algorithm in ISAC (Interaction between Structures, Aerodynamics and Controls, Ref. 8) was used to obtain the s-plane form of the unsteady aerodynamics needed in the open-loop equations of motion. Generally, the s-plane approximation is applied to all the elements of the GAF matrices, i.e., [$Q(ik)$], [$Q_c(ik)$] and {$Q_g(ik)$}, with the typical element represented by

$$Q(s) = A_0 + A_1(b/\mathrm{v})s + A_2(b/\mathrm{v})^2 s^2 + \sum_{m=3}^{6} \frac{A_m}{[s + (\mathrm{v}/b)b_{m-2}]} \tag{13}$$

The matrices A_0 through A_6 appearing in Eq. (13) represent the rational-function approximation of the s-plane aerodynamics and are evaluated by a least-squares fit of the tabular values of the generalized aerodynamic force coefficients. The quantity b in the above equation is defined as $(cref_{wtm}/2)$ and the quantities b_{m-2} are arbitrarily selected normalized lag coefficients.

Equations of Motion of a Spring-Mounted Aeroservoelastic Wind-Tunnel Model

During the HSR program, the original finite element model received from Boeing represented an unsupported, free-free, full-sized TCA aircraft configuration. However, the proposed wind-tunnel model of the TCA configuration is configured to be spring mounted in the wind tunnel. The easiest and the most adaptable approach to accommodate the spring mounting system modeling is to include a matrix term in the generalized modal coordinates into the free-free, wind-tunnel aeroelastic EOM. This approach allows easy changes of the spring stiffness parameter in the numerical simulation of the aeroelastic wind-tunnel model. Furthermore, it avoids the much more difficult task of regenerating the aerodynamics and the aeroelastic EOM, if, instead, the spring constants were changed in the FEM.

The basic form of the first-order open-loop ASE equation appearing below is the same as the one given in Reference 7. If the basic form of the state-space equation is modified to include the term representing the spring-mounting system, then the state-space equation of the wind-tunnel model is given by

$$\begin{Bmatrix}\dot{x}_1\\ \dot{x}_2\\ \dot{x}_3\\ \vdots\\ \dot{x}_6\end{Bmatrix}=\begin{bmatrix} 0 & I & 0 & \cdots & 0\\ -\overline{M}^{-1}(\overline{K} & \overline{D} & \overline{q}I & \ldots & \overline{q}I)\\ 0 & A_3 & -Ib_1 & 0 & 0\\ \vdots & \vdots & 0 & \ddots & \vdots\\ 0 & A_6 & 0 & 0 & -Ib_4\end{bmatrix}\begin{Bmatrix}x_1\\ x_2\\ x_3\\ \vdots\\ x_6\end{Bmatrix}+\begin{bmatrix} 0 & 0 & 0\\ \overline{M}^{-1}(\overline{K}_c & \overline{D}_c & \overline{M}_c)\\ 0 & A_{c3} & 0\\ \vdots & \vdots & \vdots\\ 0 & A_{c6} & 0\end{bmatrix}\begin{Bmatrix}u_c\\ \dot{u}_c\\ \ddot{u}_c\end{Bmatrix}$$

$$+\begin{bmatrix} 0 & 0\\ \overline{M}^{-1}(& \overline{K}_g \quad \overline{D}_g)\\ 0 & A_{g3}\\ \vdots & \vdots\\ 0 & A_{g6}\end{bmatrix}\begin{Bmatrix}w_g\\ \dot{w}_g\end{Bmatrix}+\begin{bmatrix} 0\\ -\overline{M}^{-1} \quad [F_{sprgLoc}]\\ 0\\ \vdots\\ 0\end{bmatrix}[K_{sprgconst}]\,[F^{T}_{sprgLoc} \quad 0 \quad 0 \quad \cdots \quad 0]\begin{Bmatrix}x_1\\ x_2\\ x_3\\ \vdots\\ x_6\end{Bmatrix} \tag{14}$$

Within the last term in the above equation, the stiffness matrix, [*Ksprgconst*], contains the spring stiffness constants as diagonal elements. These constants can easily be changed as simulation parameters, when the above equation is implemented in a numerical simulation. Also in the last term, the quantity, $F_{sprgLoc}$, which is modal deflections in the vertical direction at the spring attachment points, provides the similarity transformation of stiffness matrix into the modal generalized coordinates.

The output equation for the vertical acceleration has the form

$$\ddot{z}=F_d\left(-\overline{M}^{-1}\begin{pmatrix}\overline{K} & \overline{D} & \overline{q}I & \cdots & \overline{q}I\end{pmatrix}\begin{Bmatrix}x_1\\ x_2\\ x_3\\ \vdots\\ x_6\end{Bmatrix}-\overline{M}^{-1}\begin{pmatrix}F_{sprgLoc} & 0 & 0 & \cdots & 0\end{pmatrix}[K_{sprgconst}][F^{T}_{sprgLoc}]\begin{Bmatrix}x_1\\ x_2\\ x_3\\ \vdots\\ x_6\end{Bmatrix}\right.$$

$$\left.+\overline{M}^{-1}(\quad \overline{K}_c \quad \overline{D}_c \quad \overline{M}_c)\begin{Bmatrix}u_c\\ \dot{u}_c\\ \ddot{u}_c\end{Bmatrix}+\overline{M}^{-1}(\overline{K}_g \quad \overline{D}_g)\begin{Bmatrix}w_g\\ \dot{w}_g\end{Bmatrix}\right) \tag{15}$$

where $\overline{M}=M+\overline{q}(b/\mathrm{v})^2A_2$, $\overline{K}=K+\overline{q}A_0$ and $\overline{D}=D+\overline{q}(b/\mathrm{v})A_1$. $\overline{M}$, $\overline{K}$, and $\overline{D}$ are the generalized mass, stiffness, and damping matrices, respectively, including the effects of the unsteady aerodynamics.

The angular rate and displacement output equations are simply

$$\dot{r}=F_r x_2 \tag{16}$$

$$z=F_d x_1 \tag{17}$$

Equations (16) and (17) are analogous to (2) and (3), except that x_2 and x_1 are the state vectors of the generalized rate and displacement, respectively.

Results and Discussion

This section consists of several components of a study to exercise the scaling process. First, a description of the finite element model is provided. Second, a brief outline is given of the steps needed to complete the solid-lined path of Figure 2. Third, root-locus results of the open-loop first-order aeroelastic EOM are shown for a wind-tunnel model and a full-sized vehicle. Fourth, a description is given of a time-domain simulation that demonstrates a closed-loop control system to suppress flutter and improve ride quality.

Finite Element Model of the Full-Sized Vehicle

Under a contract to NASA Langley Research Center, Boeing-Long Beach developed an MSC.Nastran flutter analytical model based on the Technical Concept Aircraft (TCA) (Ref. 9). A semi-span FEM of a strength-sized TCA was used as the basis for a wind-tunnel model. To accommodate the anticipated additions of instrumentation and other hardware in the physical wind-tunnel model, the distributed mass of the fuselage was arbitrarily assumed to be twice as large as in the full-scaled aircraft. This additional mass had no significant effect on the critical flutter mode.

The only modifications made to the FEM received from Boeing were the additions of a chin fin and a ride control vane. The 9,500 node semi-span finite element model is

shown in Figure 3, where the accelerometer locations and control surfaces relevant to this study are indicated. Although many more accelerometers are usually used when testing aeroelastic models, the accelerometers indicated are the only ones proposed for the active control system of the wind-tunnel model.

Generating the Aeroservoelastic Analytical Model

Using the full-sized, semi-span aeroelastic FEM of the TCA, MSC.Nastran analyses were performed initially to generate the prescribed rigid-body and control surface mode shapes needed for flight control applications. Using DMAP, these mode shapes were then combined with the flexible modes in the MSC.Nastran Aeroelastic Response Analysis and used to generate and output the generalized mass matrix, the natural frequencies, the frequency-dependent GAF matrices, and the modal sensor deflections.

Table 2 gives the target model size, the dynamic pressure (near flutter), and the speed of sound for the test medium selected for the proposed wind-tunnel aeroelastic model and the corresponding values for the full-sized flight vehicle. Based on the values of Table 2 and the scale factor equations of Table 1, Table 3 contains the computed values of the scale factors used to develop the desired analytical model.

With the scaling rules given in the Implementation of the Scaling Method section, the matrices that were output by the Aeroelastic Response Analysis are then scaled by the scale factors given in Table 3. As a product of the scaling process, some values of some of the key physical quantities are given in Table 4.

Finally, the first-order space-space aeroservoelastic equations are formed using the procedure and equations given in the Analytical Model section**.**

Open-Loop Root Locus Analysis

An example problem was constructed to check the scaling rules for the open-loop aeroelastic EOM. If successful, this example problem will predict the correct root-locus pattern with increasing dynamic pressure of the scaled wind-tunnel model. Furthermore, if the root-locus patterns scale correctly, then, of necessity, the respective flutter frequencies and the respective flutter dynamic pressures will also scale correctly.

All the eigenvalues results at the various dynamic pressures for both the vehicle and the scale model were computed at a single analysis condition of 0.95 Mach number and with a 0.02 structural damping applied to the flexible modes. Figure 4 contains the vehicle root locus at the seven dynamic pressures indicated in Table 5. Figure 5 contains the scaled wind-tunnel model root locus at the dynamic pressures also indicated in Table 5. Both figures show only the first seven modes of the respective state-space aeroelastic EOM that contain two rigid-body and 20 flexible modes.

Careful inspection of Figure 4 and 5 reveals that the root-locus pattern for the full-sized TCA and the root-locus pattern for the scaled wind-tunnel model are identical. For each corresponding pair of eigenvalues from Figure 4 and Figure 5, the ratio of the magnitudes of real part to real part and imaginary part to imaginary part is identically equal to the frequency scale factor. This agreement constitutes a successful check of the scaling process.

Time Simulation of Closed-Loop TCA Wind-tunnel Model

This section of the paper employs the ASE EOM of the scaled wind-tunnel model to perform selected time-domain numerical simulations. These simulations are typical of those that might be performed before the wind-tunnel model is designed and built. They actually include investigations of model responses under various closed-loop conditions.

A Simulink model (Ref. 5) was developed for the purpose of performing time simulations of the semi-span wind-tunnel model of the TCA with an active control system. The Simulink block diagram of the simulation model is given in Figure 6. The top portion of the figure shows the actuators, aeroservoelastic state-space model including the spring mounting-system modeling, and the sensors (accelerometers), while the bottom portion shows the feedback controllers. Figure 3 shows the locations of two vertical springs for the mounting system.

Figure 7 shows the gain and transfer function blocks of the two control laws. Both control laws act as rate feedback systems with a low-pass filter to attenuate the effects of the higher frequency structural modes. The top controller in the figure is designed to stabilize the critical flutter mode and uses a vertical wing accelerometer as the sensor. Its location is near the hinge-line of outboard trailing edge flap which is used as the control effector. The bottom controller in the figure is designed to improve ride quality by reducing fuselage motions at the pilot station. This controller uses a vertical accelerometer near the pilot station as the sensor and the ride control vane just forward of the pilot station as the control effector.

The locations of all the accelerometers and control effectors are shown in Figure 3. The horizontal tail as indicated in the figure is the third control surface and its function is to provide disturbance inputs into the model.

To demonstrate the flutter mode stability augmentation and ride quality control systems, several time histories resulting from applying a doublet excitation via the

horizontal tail are presented. Figure 8 shows the time history of the doublet excitation signal which was used to excite both the open- and closed-loop simulation models. With both control loops open, at a Mach of 0.95 and at dynamic pressure of 150 psf, the model is unstable as shown in Figure 9 by the divergent time trace of the acceleration at the wing flap location. This simulation result confirms the unstable root in the plot of Figure 4.

Figures 10 and 11 show the convergent time histories of the accelerometers at the same wing flap location and at the pilot-station location, respectively, indicating a stable system when the two loops are closed. In Figure 12 and 13, only the flutter suppression loop is closed. From the likeness of Figures 10 and 12, the ride quality control law appears to have very little effect on the response of the wing. In comparing the accelerations of Figures 11 and 13, the magnitude of peak negative accelerations at the pilot station is increased by 33% by opening the loop of ride quality control law.

Concluding Remarks

A method of scaling was described to obtain the aeroelastic equations of motion of a wind-tunnel model. To implement this method, a set of simple scaling rules involving the modal matrices were given to aid in transforming the full-sized aircraft aeroelastic equations of motion to that of a wind-tunnel model. This approach avoids proceeding with a complicated set of scaling rules to scale a multitude of discrete coordinate equations of motion of a detailed finite element model. In addition, the manner of incorporating analytically a model support system with modal stiffness in the formulation was also provided. A full-sized, semi-span finite element model of the TCA of the HSR program was introduced to exercise the scaling process. A brief outline of the steps involved in generating the aeroelastic EOM of the full-sized vehicle, scaling process, and forming the first-order equations of motion of wind-tunnel model was also provided. The scaling process was verified by comparing the respective root-locus derived from the full-sized-vehicle aeroelastic EOM to the root locus from the scaled wind-tunnel model. Selected time-history plots from the simulation of an actively controlled wind-tunnel model were given to demonstrate the utility of the scaling process.

Acknowledgments

The author would like to thank Grant Wong for designing and providing the ride quality and flutter stability augmentation control laws for this paper while he was employed by the Boeing Company

References

1. Cole, S.; Perry, B.; and Miller, G.: *An Overview of the Active Flexible Wing Program*, Presented at Fourth Workshop on Computational Control of Flexible Aerospace Systems, Williamsburg, Va., July 11-13, 1990.
2. Rodden, W.P., and Johnson, E. H.: **MSC/NASTRAN Aeroelastic Analysis User's Guide**. The MacNeal-Schwendler Corporation, 1994.
3. Reymond, Michael: **DMAP Modules and Data Blocks**, MSC/NASTAN Version 70.7.
4. **MATLAB, Using Matlab**: Math Works, Inc., Natick, MA 01760-2098, Nov. 2000.
5. **SIMULINK Dynamic System Simulation for MATLAB**: Math Works, Inc., Natick, MA 01760-2098, Nov. 2000.
6. Bisplinghoff, R L., Ashley, H., and Halfman, R. L.: **Aeroelasticity**, Addison and Wesley Pub. Co., 1957.
7. Mukhopadhyay, Vivek; Newsom, Jerry R.; and Abel, Irving: *A Method for Obtaining Reduced-Order Control Laws for High-Order Systems Using Optimization Techniques*, NASA Tech. Paper 1876, August 1981.
8. Peele, E. L. and Adams, Jr., W. M.: *A Digital Program for Calculating the Interaction Between Flexible Structures, Unsteady Aerodynamics and Active Controls*, NASA Tech Memo. 80040, January 1979.
9. Baker, Myles L.; Lenkey, Peter and Fu, Lei: *Parameter Flutter Analysis of the TCA Configuration and Recommendation for FFM Design and Scaling*, Report CRAD-9408-TR-3342, Nov. 21, 1997.

Figure 1. Drawing of the supersonic Technical Concept Aircraft.

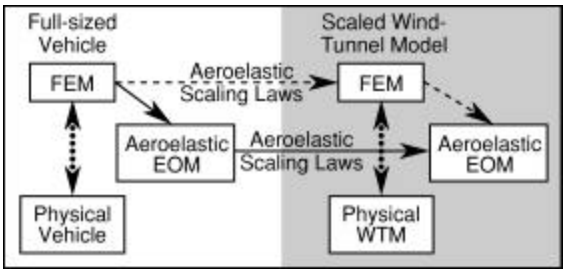

Figure 2. Flow Diagram of the possible paths for generating a wind-tunnel aeroelastic EOM.

Table 1. Description of the physical quantities, units and scale factor symbols or equations.

Physical Quantities	Units	Scale Factors
Length	l	S_l
Velocity	l/t	S_v
Dynamic Pressure	$m/(lt^2)$	S_q
Density	m/l^3	$S_r = S_q / S_v^2$
Mass	m	$S_m = S_r S_l^3$
Time	t	$S_t = S_l / S_v$
Mass Moment of Inertia	ml^2	$S_I = S_m S_l^2$
Frequency	$1/t$	$S_f = S_v / S_l$
Force	ml/t^2	$S_F = S_m S_v^2 / S_l$

Table 2. Values of the physical quantities for model in heavy gas and aircraft in air. The model values are the desired or target quantities.

Physical Quantities	Model	Aircraft
Mach	0.95	0.95
Length, ft.	16.0	326.0
Flutter dynamic pressure, psf	125.0	450.0
Speed of Sound, fps	548.0	1026.0

Table 3. Description of the physical quantities, symbols, and values of the different scale factors.

Physical Quantity	Scale Factor	Value
Length	S_l	0.0491
Velocity	S_v	0.5341
Dyn. Pressure	S_q	0.2778
Density	S_r	0.9737
Mass	S_m	1.151×10^{-4}
Time	S_t	0.0919
Mass Moment of Inertia	S_I	2.773×10^{-7}
Frequency	S_f	10.88
Force	S_F	6.691×10^{-4}

Table 4. Values of physical quantities for model in heavy gas and aircraft in air. Model values are derived from scaling process.

Physical Quantities	Model	Aircraft
Half Mass, lb.	50.23	436445.
1st Mode Freq., Hz.	12.087	1.11
Flutter Freq., Hz.	17.2	1.58
Ref. Length, in.	14.88	303.035

Table 5. TDT and equivalent TCA flight conditions at which roots were evaluated for open-loop plant model root locus analysis.

Wind-Tunnel Model Conditions Mach No. = 0.95, Velocity = 520.6 fps	Equivalent TCA Flight Conditions Mach No. = 0.95, Velocity = 974.7 fps
Dynamic Pressure, psf	Dynamic Pressure, psf
50.	180.
75.	270.
100.	360.
125.	450.
150.	540.
175.	630.
200.	720.

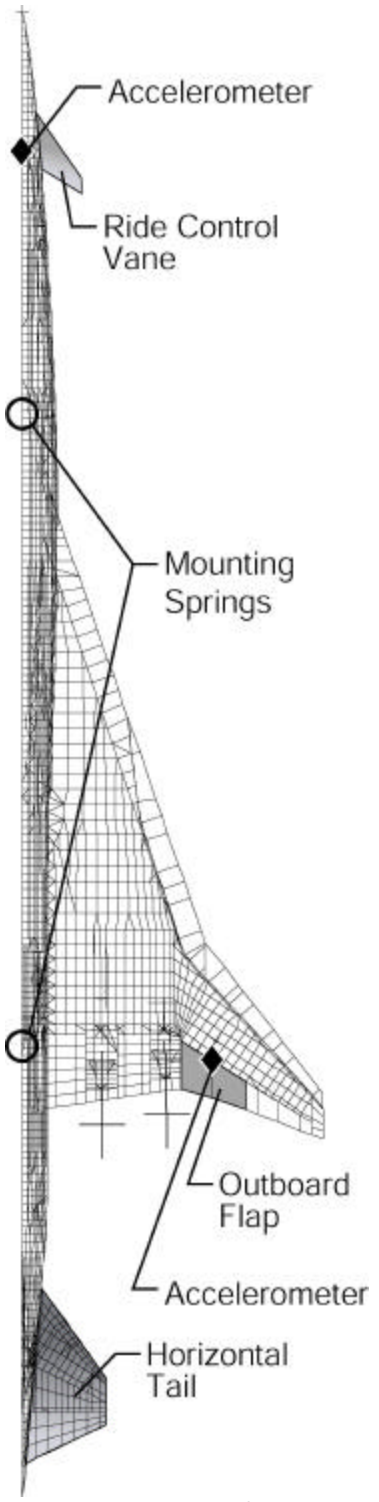

Figure 3. Semi-span finite element model of the TCA with relevant accelerometer, control surface and mounting spring locations indicated.

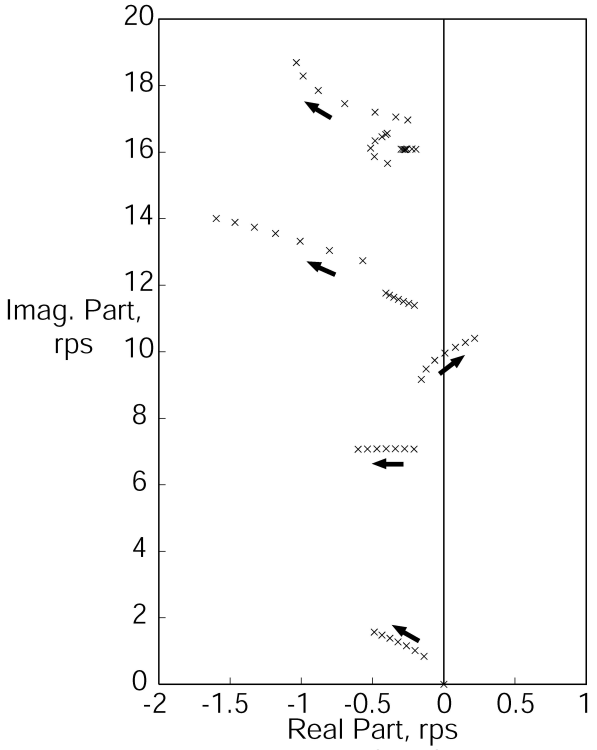

Figure 4. Open-loop root locus of the full-sized TCA with respect to dynamic pressure at Mach = 0.95 and velocity of 974.7 fps.

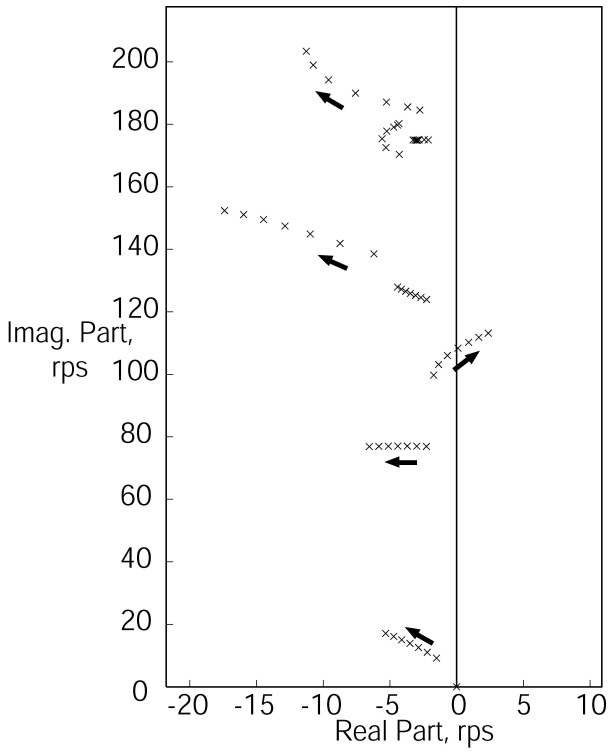

Figure 5. Open-loop root locus of the wind-tunnel model with respect to dynamic pressure at Mach = 0.95 and velocity of 520.6 fps.

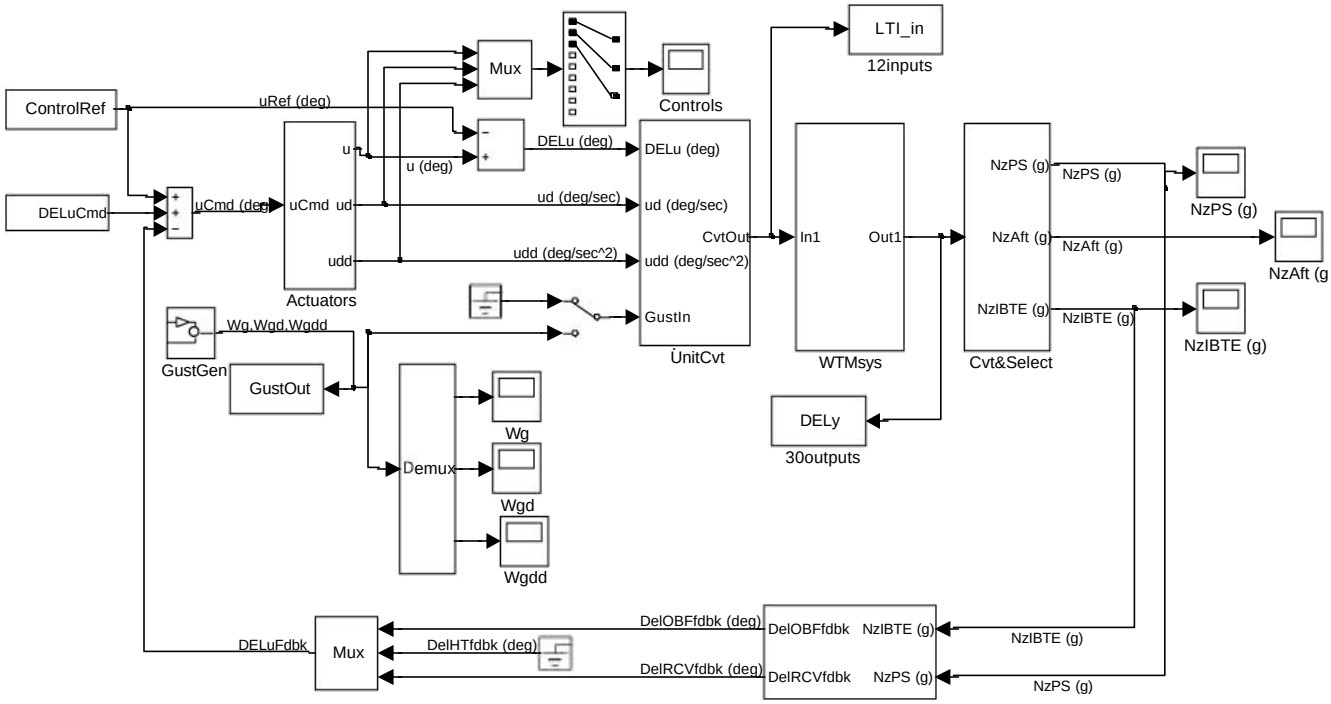

Figure 6. Simulink model of the TCA wind-tunnel model with control system.

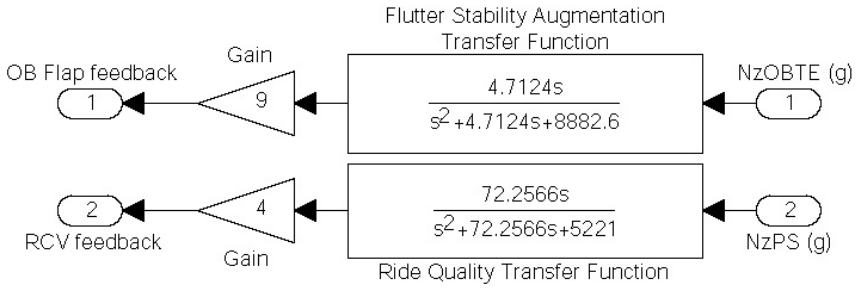

Figure 7. Flutter stability augmentation and ride quality control laws.

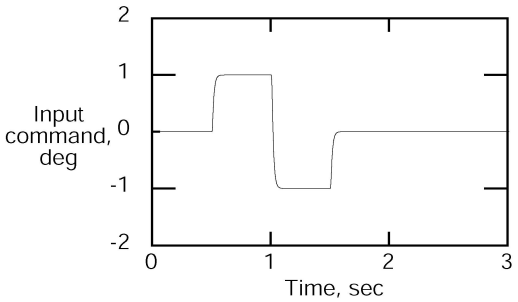

Figure 8. Horizontal tail input command, M = 0.95 and $\bar{q}$ = 150 psf.

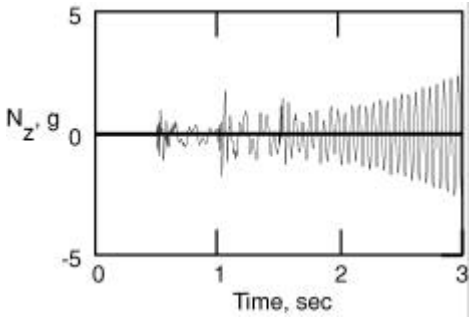

Figure 9. Wing acceleration under open-loop conditions, M = 0.95 and $\bar{q}$ = 150 psf.

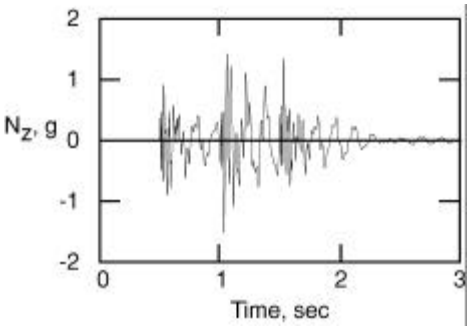

Figure 10. Wing acceleration with both loops closed, M = 0.95 and $\bar{q}$ = 150 psf.

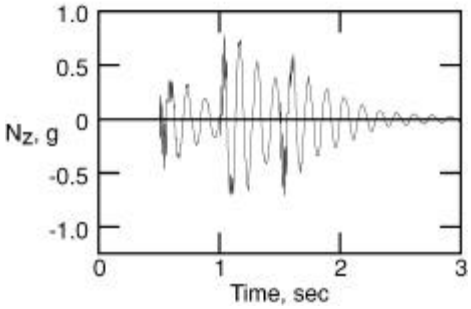

Figure 11. Pilot station acceleration with both loops closed, M = 0.95 and $\bar{q}$ = 150 psf.

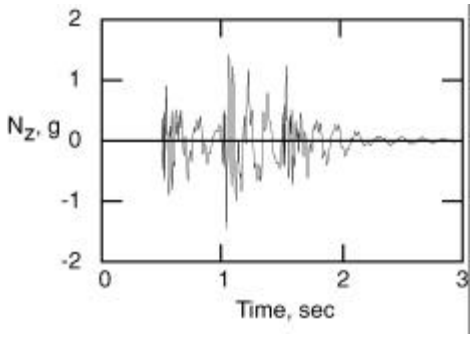

Figure 12. Wing acceleration with flutter suppression only, M = 0.95 and $\bar{q}$ = 150 psf.

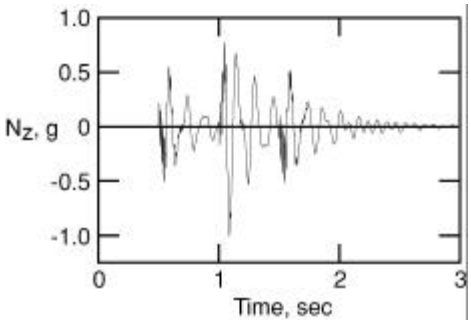

Figure 13. Pilot station acceleration with flutter suppression only, M = 0.95 and $\bar{q}$ = 150 psf.